The electronic structure of an artificial electronic Lieb lattice

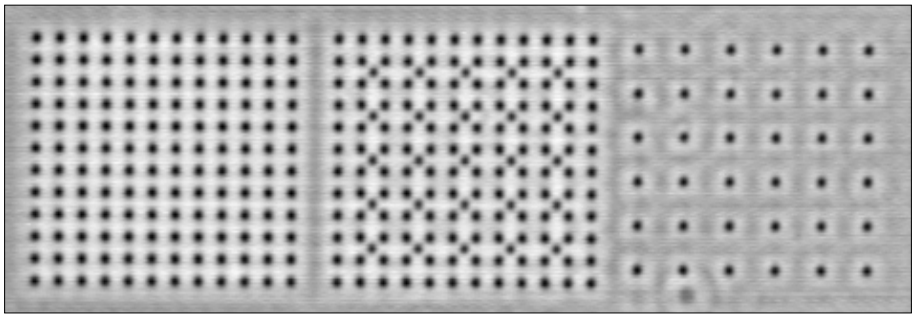

Thomas Gardenier, B.Sc.

Condensed Matter and Interfaces
Debye Institute of Nanomaterials Science
Utrecht University

Supervisors:
Marlou Slot M.Sc.
Dr. Ingmar Swart
Prof. dr. Daniël Vanmaekelbergh

Master's thesis — December 15, 2016

Abstract

The honeycomb lattice of carbon atoms forming graphene has many interesting properties including a remarkable electronic band structure. In the band structure the valence and conduction band touch forming a so-called Dirac cone, a linear energy-momentum dispersion. The square-depleted lattice, or Lieb lattice, has one corner and two edge sites per unit cell in a significantly different geometry to graphene but also contains Dirac cones in its bandstructure. In this case there is also a third, flat, band intersecting the Dirac cone at the Fermi energy. This flat band is localised on the two edge sites of the unit cell while the corner sites onlycontribute to the top and bottom bands converging into a Dirac cone. The band structure of the Lieb lattice has, however, never been measured and proved in an artificial electronic lattice. In this thesis we show the experimental realisation of constructing and measuring an artificial electronic Lieb lattice made by nano-scale patterning of a two-dimensional electron gas. CO molecules were manipulated on a Cu(111) surface to create a Lieb lattice in the existing surface state. By performing scanning tunneling spectroscopy and differential conductance mapping we confirmed the localisation of the wavefunctions contributing to the bandstructure which is shown to be different for the states contributing to the flat band and the states contributing to the upper and lower bands converging to a Dirac cone. We show further that changes in the unit cell size can tune the energy of the band structure. We also investigated the higher-energy effects encountered in the bandstructure. These results could be used for further investigations into the possibilities to tune the electronic structure of nano-patterned surface states.

Cover figure: Scanning tunneling microscope image of an ordered group of 349 CO molecules all manipulated laterally into place by hand forming three different lattices. **(Left)** *12 by 12 square lattice with a unit cell of 1.33 by 1.28 nm.* **(Centre)** *5 by 5 Lieb lattice with surrounding wall with a unit cell of 2.66 by 2.56 nm.* **(Right)** *5 by 5 square lattice with a unit cell of 2.66 by 2.56 nm. Dimensions of the figure are 20 by 50 nm.*

Contents

1 Introduction

True two-dimensional materials of one atom or molecule thick are novel materials that have attracted a lot of attention in the last decade. This is mainly due to graphene, a one-atom thick carbon honeycomb lattice with fascinating properties discovered in 2004 [1]. Some interesting properties of graphene arise from the extraordinary band structure which consists of two touching bands forming a so-called Dirac cone [2]. A Dirac point is where two bands touch forming a cone because the dispersion has a linear energy-momentum relation in reciprocal space.

Not only hexagonal structures can have a Dirac cone, the Lieb lattice has it too [3]. However, the Lieb lattice has an extra interesting feature in the band structure, a flat band intersecting the Dirac cone. A flat band indicates a high density of states in a very narrow energy range while also theoretically leading to zero conductivity at the Dirac point [4]. The dispersionless band is also interesting in the field of topology [5] although this will not be discussed in this thesis .

To investigate the band structure of a Lieb lattice one has to create a two-dimensional Lieb lattice first as the lattice has never before been reported to exist as a physical lattice in nature. Various research groups have used different approaches to construct such an artificial lattice. Two examples include the cold atom approach [6, 7] and photonic lattices [8]. However, these methods do not create an electronic lattice. Gomes *et al.* successfully synthesized the first artificial electronic lattice, a molecular graphene system assembled by manipulating carbon monoxide molecules on a two-dimensional electron gas on a copper surface in a scanning tunneling microscope (STM) [9]. The measurements of the band structure were performed in-situ by scanning tunneling spectroscopy and differential conductance maps. As the tunnelling conductance can be related to the (local) DOS, it is a crucial tool for investigation of electronic band structures in the STM.

In this research we want to create an electronic Lieb lattice by lateral manipulation of CO molecules evaporated on to Cu(111) [10, 11] and subsequently measure its electronic structure while relating the experimental results to theoretical calculations.

By creating an artificial lattice in the STM we can measure the electronic structure of the lattice immediately after completion. Due to the ability to modify such artificial lattices this research opens up new pathways to change parameters in a system inducing superconductivity [12], spin-orbit coupling [13] or the fractional quantum hall effect [14] effectively broadening the range of materials one can investigate.

2 Theory

In this chapter there will be a short description of the Lieb lattice and its electronic structure, the sample and its properties, measurement techniques and DFT on the system.

The Lieb lattice is a line-centered square lattice [5], or square-depleted lattice, with three equivalent sites in the unit cell as shown in Figure 1a. The edge sites (A and C) are different to the corner sites (B) when comparing neighbours. The edge sites have only two neighbouring sites while the corner sites have four neighbours. The Lieb lattice has garnered much interest due to an unusual band structure with the presence of a topological flat band intersecting a Dirac cone [7, 15] (Figure 1b). In a Dirac cone the electronic band structure has a linear dependence on the wavevector k instead of the expected square dependence [16]. A well-known example of a material exhibiting Dirac cones is the honeycomb lattice of graphene where due to the Dirac cone, electrons travel ballistically [17]. The Lieb lattice is however most definitely not a honeycomb structure, but also shows a Dirac cone in reciprocal space. The Lieb lattice has a different geometry than graphene, so in reciprocal space the Dirac cone appears at the M-point instead of the K-point.

Many papers have investigated the electronic structure of a Lieb lattice using tight-binding and other methods [3, 5, 19], and some even subsequently propose how to make an electronic Lieb lattice in the STM [20]. However, no one has experimentally proved the existence of an artificial electronic Lieb lattice. Photonic Lieb lattices have been created [8, 21] and measured proving the existence of the Lieb band structure, however they are not electronic. When using photonic lattices there are no electrons but photons at the three lattice sites and therefore the properties of such a lattice will not be comparable to real lattices made from atoms. Effectively an atom is a collection of electrons surrounding a nucleus, so to make an artificial electronic Lieb lattice one must use a method that enables electrons to be in the position of the Lieb lattice nucleus sites.

2.1 Theoretical approach

Using a three-site model we can perform tight-binding calculations on the Lieb lattice. The calculations produce a bandstructure as shown in Figure 1b. Here we see the Dirac points with linear energy-momentum dispersions intersected by the flat band. The density of states of this bandstructure is shown in Figure 1c where the flat band (in green) generates a very high, sharp peak at the Fermi energy, precisely in the middle of the two bands (in blue) that converge to the Dirac cone. The flat band DOS is only generated by states localised on the edge sites meaning that the states at the Fermi energy are effectively forming a square electronic crystal. The upper and lower bands contain states located on both corner and edge sites where the corner sites have a higher intensity. This is, however, all true for a nearest-neighbour approximation. When including real effects such as next-nearest-neighbour interactions the relative intensities and positions of these three interesting features change as can be seen in the muffin-tin potential calculation shown in Figure 1d. Most notably the density of states of the flat band broadens due to corrugation appearing in the flat band. This is however not the scope of this thesis. Also,

because we cannot build perfect periodic and infinite lattices, the effects of building a finite lattice are including in this calculation. The upper band contributing to the Dirac cone gains intensity in comparison to the lower band, while an extra peak appears in the

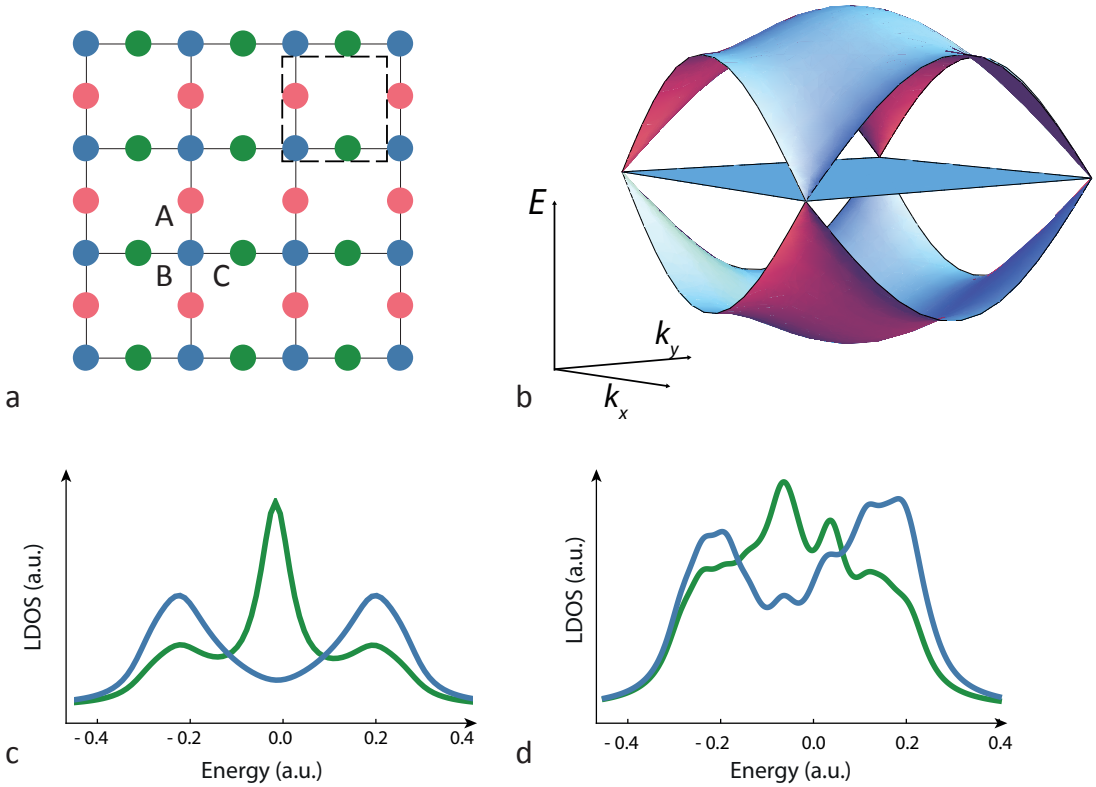

Figure 1: Description of the Lieb lattice **(a)** Schematic representation of the Lieb lattice with three sites (A, B and C) per unit cell (dashed black square). Sites A and C are equivalent edge sites, both having two neighbouring sites while B is a corner site with 4 nearest neighbours. **(b)** Band structure of the Lieb lattice in a nearest-neighbour tight-binding approximation with k_x and k_y in the horizontal plane as a function of energy. The band structure consists of three bands of which the top and bottom band touch at the M points in reciprocal space forming a Dirac cone intersected by the third, dispersionless band. **(c)** Nearest-neighbour tight-binding calculation of the local density of states of the edge sites (green) and corner sites (blue) of a Lieb lattice as a function of energy. Realise that the relative intensities of (c) vary slightly due to discretisation of the band structure. For example, the high DOS of the flat band is in principle a delta function, but is portrayed with an artificial broadening. **(d)** Muffin-tin calculation of the local density of states of the edge sites (green) and corner sites (blue) of a finite Lieb lattice as a function of energy. Note the change in relative intensities of the corner site spectrum and the extra peak in the edge site spectrum. We included a broadening of 80 mV for the muffin-tin model. Adapted from [18].

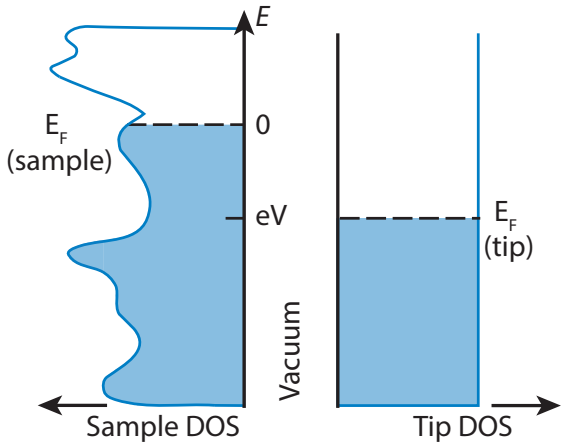

Figure 2: The principle of the scanning tunneling microscope. On the left and right are the densities of states of the sample and tip respectively. In the centre a vacuum barrier (UHV) is situated creating a potential barrier for the tunnel current. The energy states are filled to the Fermi energy E_F. A tunnel current can flow from the sample to the tip by applying a negative bias voltage to the tip or a positive bias voltage to the sample. Figure adapted from [24].

edge spectrum at slightly higher energies than the flat band itself.

2.2 Scanning tunneling microscopy

Scanning tunneling microscopy (STM) is a very versatile technique developed in 1982 by Binnig and Rohrer [22]. Generally seen, this technique consists of an atomically sharp sharp needle, or tip, scanning over a conductive surface while measuring the tunnel current going from sample to tip. It relies on the basic quantum mechanical principle of tunneling. Tunneling is where a particle, in this case an electron, has a non-zero probability to appear at the other side of a potential barrier. This is schematically illustrated in Figure 2. This concept is used in the STM where the ultra-high vacuum (UHV) of $\sim 10^{-10}$ mbar is the potential barrier. If the tip is very far from the sample surface the probability of electrons tunneling to the tip is virtually zero. Approaching the tip to ranges of several nanometers increases the current exponentially with the distance to a few hundred pA or tens of nA. The standard setting for the STM is in a feedback loop linked to the tunneling current. Applying a certain bias voltage over the tip and sample generates a tunnel current. The feedback loop maintains the current setting, if it becomes too low, e.g. due to a CO molecule with very few electrons at the bias voltage, the feedback mechanism approaches the tip to increase the probability of tunneling and thus the tunnel current. If the current becomes too high, the tip is retracted. A molecule, or system has multiple energy levels, or bands. Reversely if the bias voltage applied over the tip and sample is in resonance with such a band or energy level, the tunnel current will be much higher than when not in resonance [23].

Scanning tunneling spectroscopy

Scanning tunneling spectroscopy (STS) is a technique to measure the differential conductance as a function of the voltage at a certain position on your sample. During a spectrum the voltage is swept from a starting voltage (e.g. 1 V) to an end voltage (-1 V) and back again. This gives a current versus voltage or I(V) spectrum. The derivative of this signal gives a $\mathrm{d}I/\mathrm{d}V$ signal which is proportional to the local density of states (LDOS). This differential is acquired using standard lock-in techniques.

The spectrum obtained is proportional to the LDOS of the sample and the tip [25, 26], see equation (1).

$$\frac{\mathrm{d}I}{\mathrm{d}V} \propto \rho_s(E_F - eV) \cdot \rho_t(E_F) \tag{1}$$

Where ρ_s is the DOS of the sample, ρ_t is the DOS of the tip, E_F is the Fermi energy and eV is the applied bias voltage. When the $\mathrm{d}I/\mathrm{d}V$ signal increases it means that there are more electrons tunnelling at that certain energy. This corresponds to a higher availability of electrons meaning a higher density of states. Due to a spectrum being taken at a single point it is a local DOS (LDOS). Because only the DOS of the sample is desired one has to remove the DOS of the tip and Cu surface. This is done by dividing the spectrum by an average spectrum taken on bare Cu(111) with the same tip as used for the measurements on the lattice. Spectra taken on Cu(111) differ with each set of measurements due to a different configuration of the tip. This also shows how important it is to divide the spectra taken on the lattices by the 'correct' Cu(111) spectrum to be able to compare the edge and corner spectra effectively.

Differential conductance maps

A differential conductance map is a scan taken at constant height with a certain applied bias voltage. Such a map visualises the localisation of certain states in the system, at the voltage applied, and thus the wavefunctions. A stack of maps taken at various energies is in principle equivalent to many spectra taken at each point in the grid and slicing them at a certain energies. A map visualises the LDOS better than spectra because the spatial resolution is inherent in a map. Also the relative intensities are visualised by the contrast in an effective way.

2.3 Cu(111) surface patterned by CO molecules

A large benefit of the STM is that you can manipulate the substrate to create a system you want to measure, and measure it immediately afterwards. Due to an electronic lattice needing electrons at the lattice sites the creation of an artificial electronic lattice requires having electrons available in the locations where one would expect the sites of the lattice. To do this we use the surface state of a clean and atomically flat Cu(111) crystal. The surface state exists in the bulk bandgap of metals and is located at the surface of a terminated crystal [25, 27]. A single copper crystal can be described by a nearly-free electron model in the bulk, but at the surface of a crystal the wave functions

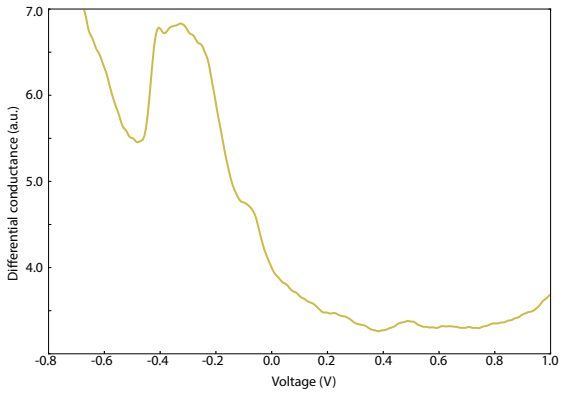

Figure 3: Representative copper spectrum taken on bare Cu(111) with the surface state visible at -0.45 V.

of the electrons suddenly have a vacuum to deal with instead of neighbouring Cu atoms. This surface state has a very sharp onset at -0.45 V [26], see Figure 3 for an example of a Cu(111) spectrum visualising the surface state. Due to the surface state there is a relatively high concentration of electrons at the surface forming a so-called two-dimensional electron gas or 2DEG.

Adding surface modifications to the 2DEG induces modulation of the electron gas and can force, or guide, the electrons into a desirable pattern [9, 28, 29]. Many different elements or molecules can be used for surface modifications such as Xe [30], Ag [29] and CO molecules [31]. We chose to use CO molecules as scatterers based on the good manipulability and effects shown in [9, 31]. When CO molecules are placed on the copper surface they change the electron presence by diminishing the electron density in their immediate surroundings. Therefore we have to place the CO molecules in an anti-Lieb lattice pattern so that the electrons of the 2DEG are located at the Lieb lattice sites. We do this in a way shown in Figure 4. Here we see the Lieb lattice in (a) with the three sites per unit cell. In (b) we see the placement of CO molecules in a cross shape which gives the electron density a kinetic deformation [32]. Simply placing carbon monoxide molecules in the empty centre of the unit cell of the Lieb lattice would have generated a square lattice of carbon monoxide. For this inverted molecular lattice to show a similar electronic band structure as the real Lieb lattice the spacing of the carbon monoxide molecules must be carefully arranged. If the outer four CO molecules are placed too close to the central CO molecule the Lieb lattice could effectively become a square lattice. A lattice spacing that is too large will cause the electrons to lose confinement into the lattice sites. Also, as explained in section 4.4, an increase in unit cell size will yield the system nearly unmeasurable by STM due to the interesting effects dropping to energies lower than the surface state onset.

The exact placement of carbon monoxide molecules on the hexagonally arranged Cu(111) surface to create a square anti-Lieb lattice had dimensions of 2.66 by 2.56 nm and is described in more detail in section 4.4 'Influence of unit cell size'.

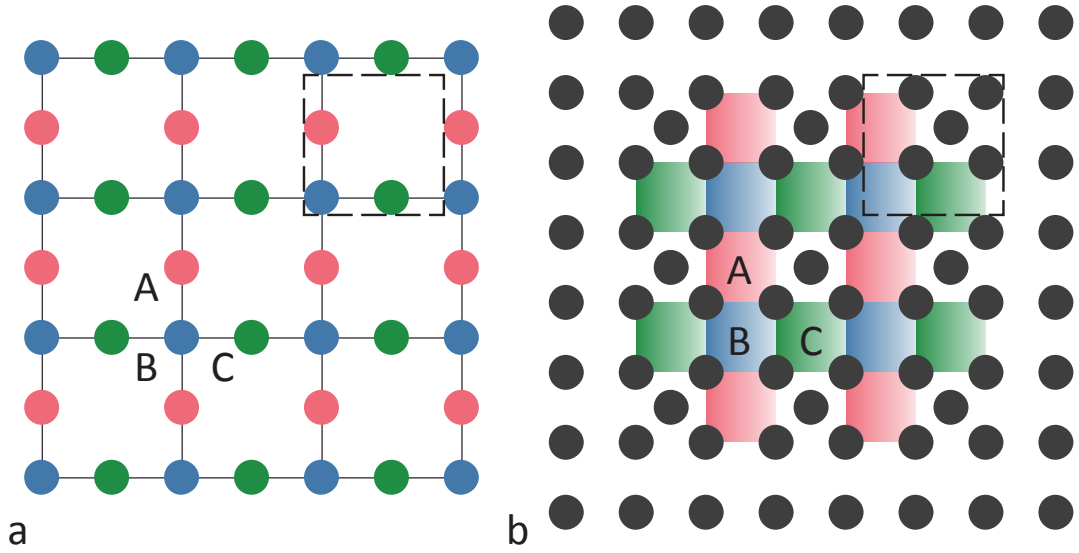

Figure 4: **(a)** Schematic representation of a finite Lieb lattice with three sites (A, B and C) per unit cell (black dashed square). Sites A and C have two nearest neighbours while site B has four nearest neighbours. **(b)** Schematic representation of a finite inverse Lieb lattice with 'crosses' of 5 CO molecules in dark grey. This pattern is expected to modify the 2D electron gas into a Lieb lattice pattern with three sites as visualised by the red, green and blue shaded areas. These areas correspond to the three sites A, B and C in the Lieb lattice.

2.4 Density functional theory

The electron densities of an inverse Lieb lattice built by placement of CO molecules on a Cu(111) surface in comparison to a clean Cu(111) surface were investigated in collaboration with Riande Dekker during the course 'Computational Quantum Mechanics' [33]. The results were not as expected on the basis of previous studies by Ropo *et al.* and Paavilaien *et al.* [34, 35], as we expected an increase in electron density between the CO molecules due to being repulsed by the negative charge of the CO. The results we found were, however, that the electron density just below and in the immediate surroundings (radius of 3 Å) of CO molecules was diminished, but that the only increase of electron density was found in deeper layers of the Cu(111). We could see no increase of electron density between the CO molecules. It might therefore be a better explanation that the CO molecules deny the electrons of the 2DEG access to the locations the molecules are located at. In this way the procedure of placing the CO molecules in an anti lattice makes much more sense.

3 Experimental Methods

3.1 Experimental setup

The measurements done for this thesis were performed in a low-temperature microscope built by Omicron Nanosciences shown in Figure 5. The microscope was cooled to 4.5 K by a cryostat filled with liquid helium and liquid nitrogen, while the pressure in the STM chamber was in the 10^{-10} mbar range. A W-tip was used which was sharpened by voltage pulses and controlled crashes into the Cu(111) surface resulting in a Cu-covered tip sharp enough to manipulate CO molecules and stable enough to take spectroscopy measurements.

For the experiments a single crystal of Cu(111) was used as substrate due to the presence of a surface state near the Fermi level creating a two-dimensional electron gas at the surface [27]. The crystal was cleaned by repeated cycles of sputtering with Ar-gas (at $3.7 \cdot 10^{-6}$ mbar) and annealing by heating the crystal to 460°C. Subsequently the sample was transferred to the LT-STM and cooled to 4.5 K. CO gas was leaked into the chamber to $2 \cdot 10^{-8}$ mbar for 3 minutes with a line of sight to the cold crystal enabling CO molecules to adsorb onto the sample.

3.2 Atom manipulation

The random position of the CO molecules adsorbed to the Cu(111) surface is far from the structure we actually want. The tip of the STM can be used to manipulate surface adsorbates to the required position [10, 36]. There are two techniques for manipulation: vertical, and lateral manipulation. We use lateral manipulation which drags or pushes the CO molecule over the surface [11] whereas vertical manipulation actually picks the molecule up and deposits it again in the required position [37]. To laterally manipulate a CO molecule to the desired position one has to approach the tip to the CO molecule by increasing the tunnel current and decreasing the bias, or gap-, voltage and move the tip to the desired location, see Figure 6a. The standard scanning parameters were a 50 mV gap-voltage with a 1 nA tunnel current setpoint, although the scan parameters are not of influence on the success rate of the lateral manipulations. One can be a lot further away from the surface (e.g. at 500 mV and 100 pA) and still get reliable manipulations.

To manipulate, the parameters are changed to 10 mV and 40 nA. The tip is closer to the surface and therefore has more interaction with the CO molecule. When moving the tip the CO molecule moves along with it [31]. The feedback loop was enabled during the manipulations. When manipulating the CO molecule one can track the Z(r) signal to see if the manipulation was successful. This signal is the tip height as a function of the distance travelled during the manipulation, see Figure 6b. Here the corresponding Z(r) signal for multiple lengths and directions of successful manipulations are shown (except for the grey line). The purple line for example shows that the CO molecule was not following a close-packed line at first, but during the second half of the manipulation is hopping from one top site of the Cu(111) surface atoms to another. All of them have equally spaced features corresponding to top, bridge and valley sites of the hexagonal

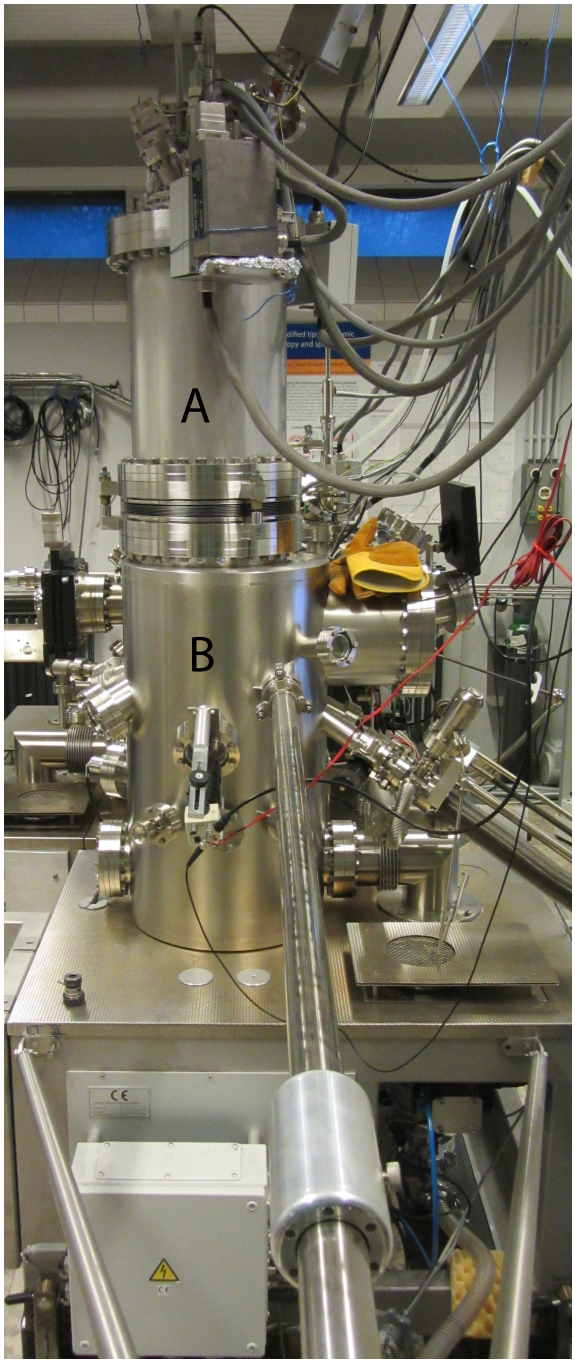

Figure 5: Scanning Tunneling Microscope used for the measurements on the Lieb lattice. **(A)** is the cryostat keeping the microscope head including tip and sample at 4.5 K. **(B)** Position of the microscope head including tip and sample.

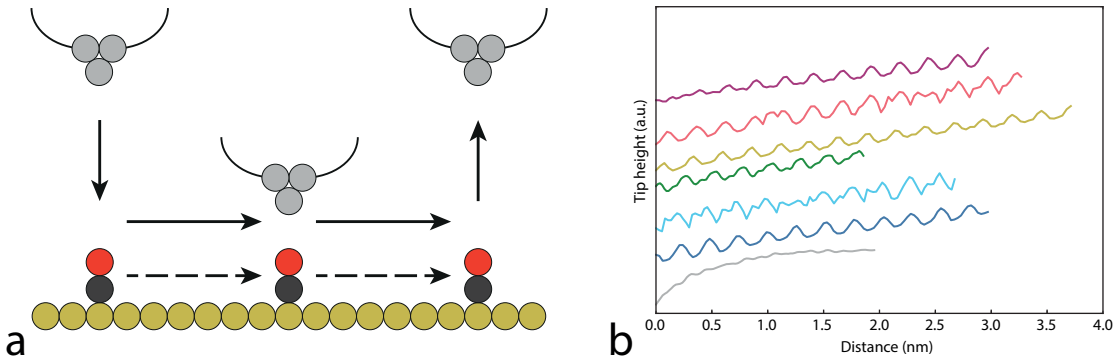

Figure 6: Lateral manipulation of CO molecules (a) Schematic representation of a lateral CO manipulation. The tip is relocated above a CO molecule after which the bias voltage is reduced to 10 mV and the tunnel current setpoint is increased to 40 nA. Both these actions approach the tip towards the CO molecule. Relocating the tip drags the CO molecule along with it, after which the tip retracts again. (b) The Z(r) signal of the tip shows the surface corrugation and thus the Cu(111) surface atoms for multiple manipulations. In grey one can see an example of a failed manipulation, where the CO molecule was not moved. All other colours correspond to successful manipulations

Cu(111) surface. One extra requirement for manipulation is most important, the tip must be sharp. Good imaging of the CO molecules generally leads to successful manipulations up to several tens of nanometres in one go.

The end position of the CO molecule after a manipulation will not always be where you expected because the molecules want to sit on top sites of the Cu(111)surface [37]. If the end of the manipulation is in between three Cu sites, it will jump to either one of them. As one can see in Figure 6b the Z(r) signals do not always end on a top site. Subsequent correction manipulations are then required. Various steps in the creation process are shown in Figure 7. In (a) we start off with a disordered pattern of CO molecules on a flat Cu(111) surface and progressing through (b)-(d) we arrive at (e) where the completed lattice is shown. The time for manual construction of a 5 by 5 Lieb lattice with surrounding walls can be as short as 5 hours.

Automating the manipulations is a natural next step, as manual manipulations become tedious rather quickly. In a similar fashion as Celotti *et al.* the decision was made to write a programme to speed up the process of building the required lattices and patterns. Ing. Stephan Zevenhuizen wrote SnapZone in Python which can take STM scans, recognize CO molecules, reposition the tip above the CO molecule and manipulate it to a pre-defined template. It also calculates the shortest paths from the CO positions to the desired positions, reducing the total manipulation time. In theory and digitally it works really well, however practically it does not as the calibration of the STM has not been corrected enough to compensate the problems of mismatching templates and reality on large scale. On a small scale of ~ 5 by 5 nm the manipulations are correct so utilising small building zones to create a large lattice should be a viable procedure.

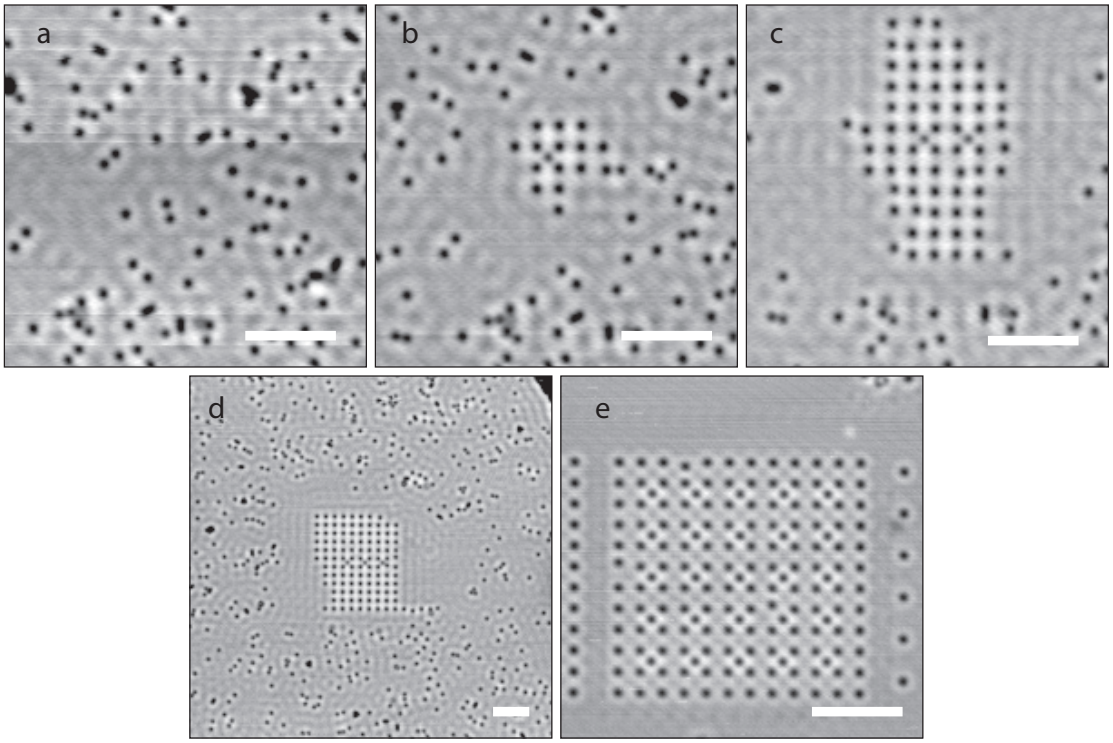

Figure 7: Height scans showing the construction of an inverse Lieb lattice. **(a)** Untouched Cu(111) surface with a random distribution of CO molecules. **(b) - (d)** Overview scans of the construction of an inverse Lieb lattice. **(e)** Final inverse Lieb lattice consisting of 169 CO molecules. Scan settings are 1 nA and 50 mV. All scale bars are 5 nm

Building a square structure on a hexagonal Cu(111) surface is not easy to start with. Unless you go to really large sizes, one cannot build a perfect square on a hexagonal lattice. We did try some close approximations as shown later in Figure 14. The nearest-neighbour distance of a Cu(111) surface is 2.556 Å [9, 38] so CO molecules must be placed at multiples of this distance (when considering close-packed rows). The most square option was a 2.66 by 2.56 nm unit cell.

3.3 Local density of states measurements

To visualise the local density of states (LDOS) many spectra were taken on various sized Lieb lattices. The spectra were taken from 1.00 V to -1.00 V with 501 points or 1.00 V to -0.70 V with 301 points and an integration time τ of 100 ms. The settings from which the spectra were started was a feedback bias voltage of 1.00 V with a current of 5 nA. The Lakeshore lock-in amplifier was set to a frequency f of 273 Hz, an oscillation amplitude A_{osc} of 20 mV rms and a sensitivity of 50 mV.

The differential conductance or $\mathrm{d}I/\mathrm{d}V$ maps were taken from -500 mV to 600 mV in steps of 50 mV resulting in 23 maps. Each map has dimensions of 18 nm by 36 nm and

was measured with 200 by 400 points using an integration time of 10 ms per point. The settings before starting the map measurements were a bias voltage of 50 mV, a current of 1 nA and a ΔZ of 0.100 nm. The maps were taken with the feedback loop disabled. The lock-in amplifier was set to a frequency f of 273 Hz, an oscillation amplitude A_{osc} of 20 mV and a sensitivity of 5 mV.

4 Results and Discussion

Many measurements have been performed on the artificial Lieb lattices. We have succeeded in measuring the electronic structure of Lieb lattices and have seen the Lieb signatures in the measurements indicating that we have succeeded in building an artificial electronic Lieb lattice. The results have been split into different aspects although frequently the various aspects came from the same set of measurements.

An artificial Lieb lattice was constructed in an inverse way as described in Chapter 3 and is shown in Figure 8. Here one can see the CO molecules in black on a Cu(111) surface. An edge and corner site are indicated by the respectively green and blue coloured circles. Note that the physical dimensions of a corner site are identical to an edge site, the difference lies purely in the number of neighbouring sites where a corner site has four edge sites as neighbours and an edge site only two corner sites.

The results will be discussed in various ways starting with spectra taken on the corenr and edge sites followed by spectra taken along a whole line within the lattice. Subsequently differential conductance maps are shown due to their power of visualisation. The effect of changing lattice parameters is discussed extensively while also higher energy states in both the square lattice and the Lieb lattice will be shown.

4.1 Scanning tunneling spectroscopy

A spectrum taken in the STM is a differential conductance, or $\mathrm{d}I/\mathrm{d}V$, plot which shows derivative of the current at each applied voltage. As mentioned in Chapter 2 the signal is proportional to the density of states of the tip and of the corresponding sample. We divide the spectra by an average spectrum taken on bare Cu(111) as shown in 'Experimental Methods'. Do realise that dividing by the Cu(111) spectrum does not create the Lieb signature, it only removes the background. The Lieb signature is always visible in the raw spectra as well.

The positions in the lattices where the spectra were taken are shown in Figure 8. The spectra taken on the square lattice are shown in red, while the spectra taken on the inverse Lieb structure are shown in blue (corner sites) and green (edge sites).

The spectra were taken between -1.00 V or -0.70 V and 1.00 V which is the region in which the local density of states is expected to change due to the presence of CO molecules [9]. The surface state of a Cu(111) surface has its onset at -0.450 V and is visible in Figure 9 as the yellow line. Different tips will change the Cu(111) spectrum, sometimes so drastically that the surface state onset is not visible anymore. Here one can see that the Cu(111) spectrum matches the shape of the spectra taken on the Lieb and square lattice quite well and can therefore be used to divide the spectra.

In Figure 9 the differential conductance spectra on a Lieb lattice and a corresponding square lattice are shown. The average copper spectrum is in yellow, the average spectra taken on the corner sites of the square lattice are in red and the average spectra taken on a Lieb corner and edge are shown in blue and green respectively. The surface state onset slope, visible in the Cu(111) spectrum around -0.45 V changes due to placement of the CO molecules [39]. In this figure we can already see intensity differences at the

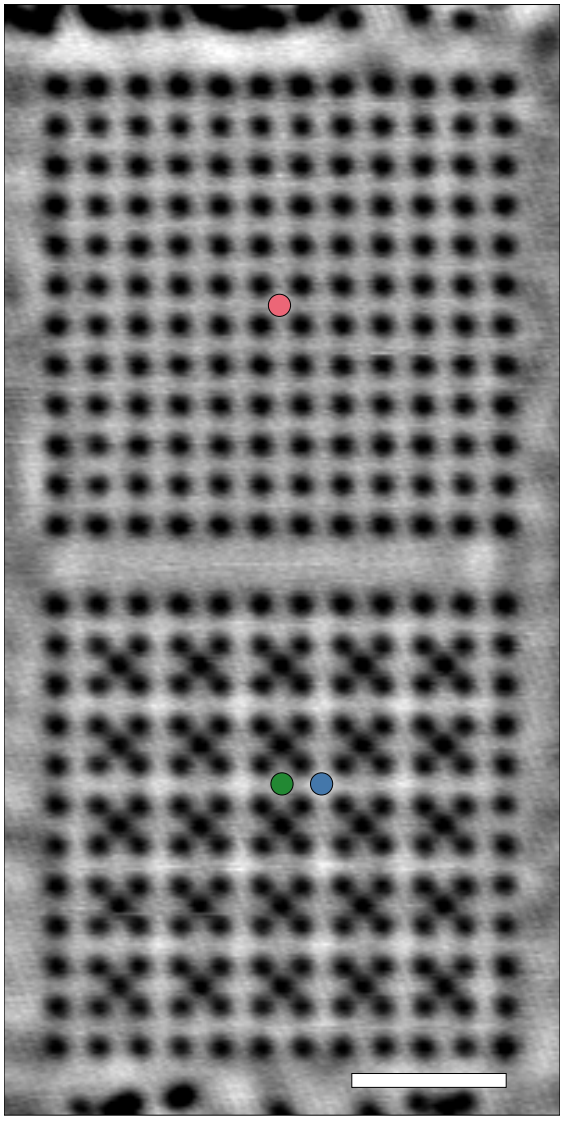

Figure 8: Arrangement of 313 CO molecules (black) into a 5 by 5 inverse Lieb lattice with a surrounding wall to increase the number of equivalent sites and a 12 by 12 square lattice. Spectra positions in the square lattice are indicated by the red circles, positions in the inverse Lieb lattice are given in blue (corner sites) and green (edge sites). The measurement settings for the scan were 1 nA and 50 mV. Scale bar is 5 nm.

energies of interest visualised by the dashed lines at -200 mV, -50 mV and 150 mV which are the same energies in Figure 10. However the density of states of the tip is still in the spectrum. To remove the effect of the DOS of the tip the spectra are divided by the Cu spectrum. The result is visible in Figure 10.

The dashed lines in Figure 10 indicate the energies of interest at -200 mV, -50 mV

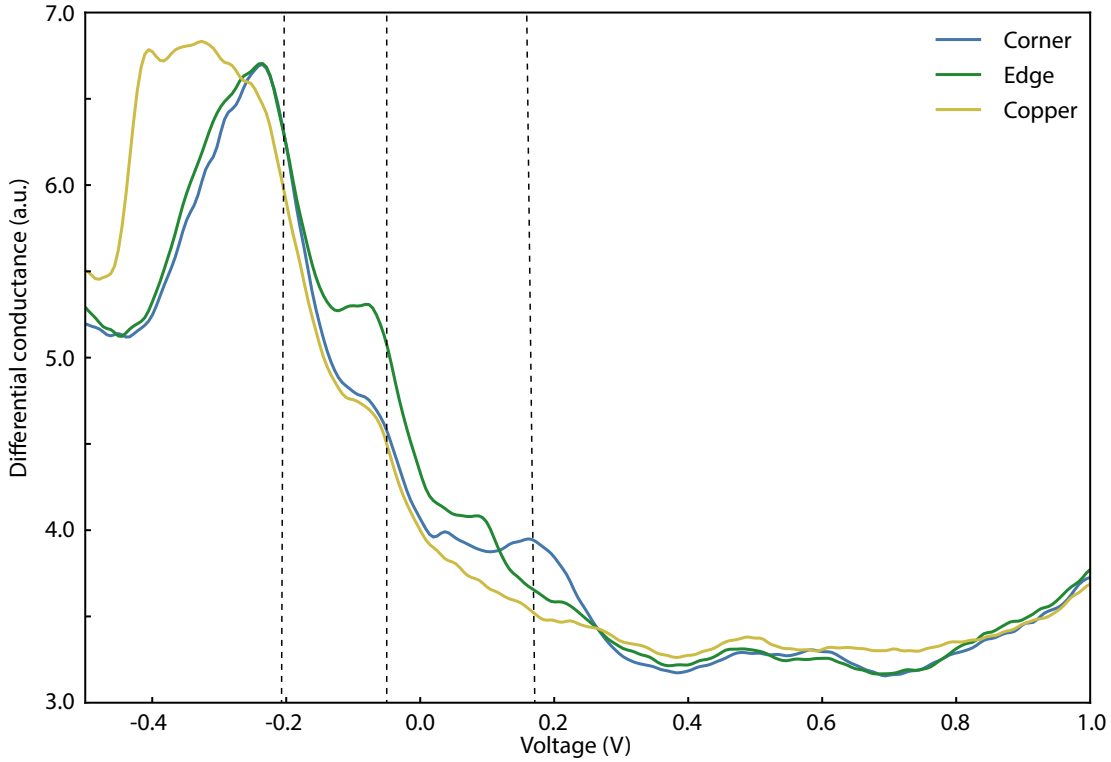

Figure 9: Raw spectra taken on Cu(111) and the Lieb lattice with the trace and retrace averaged and a small convolution filter applied to reduce noise. Dashed lines are included at the energies of interest (-200 mV, -50 mV and 150 mV) at which $\mathrm{d}I/\mathrm{d}V$ maps were taken.

and 150 mV. At these energies differential conductance maps are shown in section 4.3. The spectra for the corner sites and the edge sites differ at various points indicating the presence of an electronic Lieb lattice. At -200 mV the corner sites have a slightly higher intensity than the edge sites and again at 150 mV. At -50 mV the situation is reversed whereby the edge sites have higher intensity than the corner sites. If one compares the spectrum of the square lattice to the Lieb spectra, one can see that between -300 mV and 200 mV the square spectrum rises in a more or less straight line. The spectra on a corner and edge site in the Lieb lattice definitely do not stay straight in this region and differ drastically from each other.

An interesting effect on the spectra caused by finite size-effects is the presence of an extra peak in the edge spectrum around 100 mV. This peak can be attributed to the finiteness of the lattice [18]. In this measurement series we built an inverse Lieb lattice of 5 by 5 unit cells. This is of course far from an ideal periodic lattice which would be periodic over tens of nanometers. If we compare the experimental spectra to the muffin-tin calculation shown in Figure 1d they match really well, connecting our results with the theory.

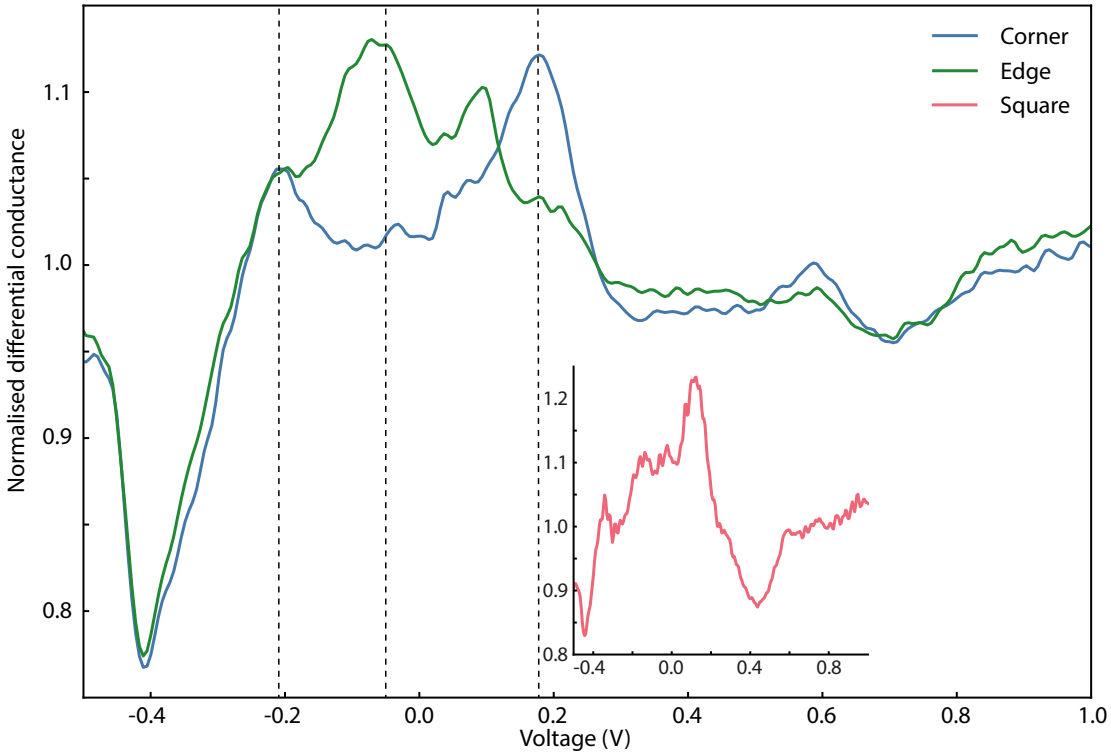

Figure 10: Spectra taken on the square and Lieb lattice divided by the corresponding Cu spectrum. This removes the tip DOS from the spectrum as well as removing any effects caused by the Cu(111) surface state. *Insert* Spectrum taken on a corner site of a square lattice with similar dimensions to the Lieb lattice.

4.2 Spectra on line

The spectra discussed in the previous section were taken on the different sites by manually positioning the tip in the centre of such a site. Spectra on line remove the small deviation induced by manual positioning by simply taking spectra on many points along a line. This enables us to visualise the transistion from a corner site to an edge site and back again. Figure 11 shows spectra when taken along a line in the Lieb lattice (a–c) or on the square lattice (d–f) used as a reference lattice. In (b) the spectra between -0.4 V and 0.2 V alternate between spectra with two peaks (corner sites) corresponding to the convergence of the top and bottom band, and one peak (edge sites) corresponding to the flat band. The two types of positions are separated by bridge sites where a high intensity is only visible around 0.55 V. Single spectra selected from the line spectra are shwon in (c). The characteristics match the locations they were measured in very well and conform nicely to the pattern such as gathered from Figure 10.

The spectra taken on a line in the small square lattice (Figure 11e) show the spectra on the corner sites. The differences between the corner spectra on the square lattice and the Lieb lattice are the same as seen in Figure 10. The corner sites on the square lattice

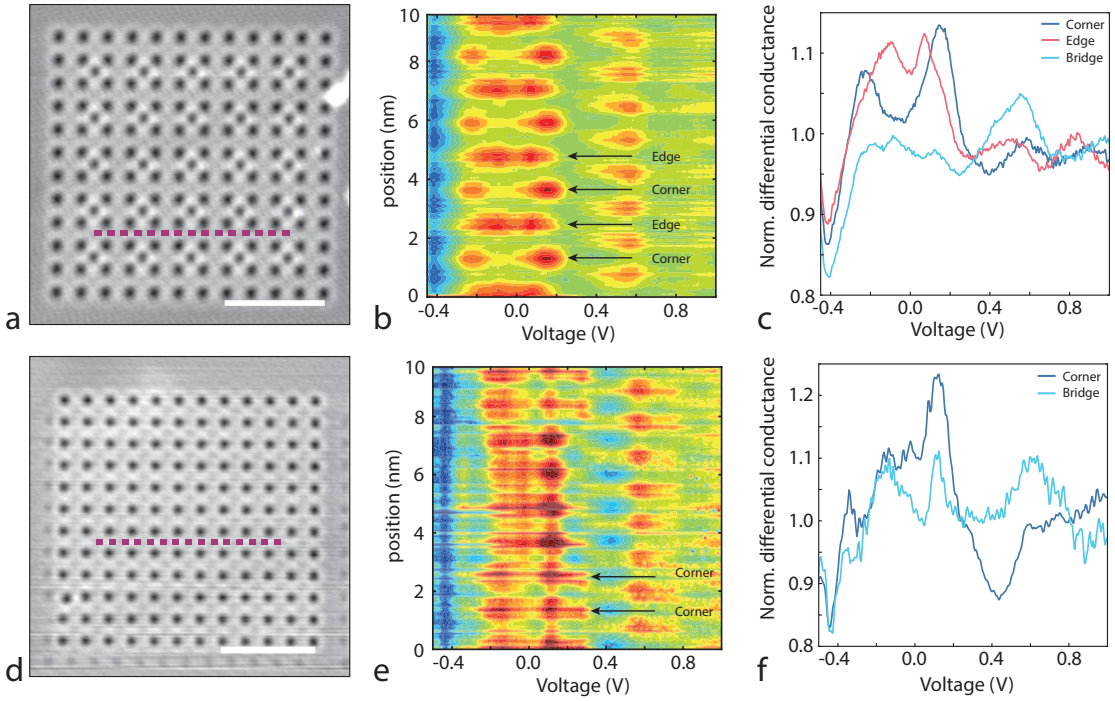

Figure 11: Line spectra **(a)** STM image of the Lieb lattice with the line along which 100 spectra were taken in purple. **(b)** Contour plot of 100 spectra taken on a Lieb lattice at the positions shown in (a). **(c)** Example of three spectra from the line spectra representative for the contour plot in (b). Spectrum taken at a corner site in dark blue, an edge site in red and a bridge site in light blue. **(d)** STM image of the square lattice with the line along which 125 spectra were taken in purple. **(e)** Contour plot of 125 spectra taken on a square lattice at the positions shown in (d) **(f)** Example of two spectra from the line spectra representative for the contour plot in (e). Spectrum taken at a corner site in dark blue and a bridge site in light blue. All scale bars are 5 nm.

have one highest intensity peak, and show no signatures of a Lieb lattice at the energies of interest.

The spectra on line certainly enhance the understanding of the difference in DOS at edge and corner sites. However, one of the best ways to visualise spatial intensity patterns is by using differential conductance mapping.

4.3 Differential conductance maps

Differential conductance maps are often a good visualisation for information about the local density of states in a system although the information contained in a stack of maps at various bias voltages is analogous to spectra taken in many places on the lattice. Figure 12 contains three maps taken at three energies which confirm the characteristics of the electronic structure of a Lieb lattice: the flat band only contains states localised

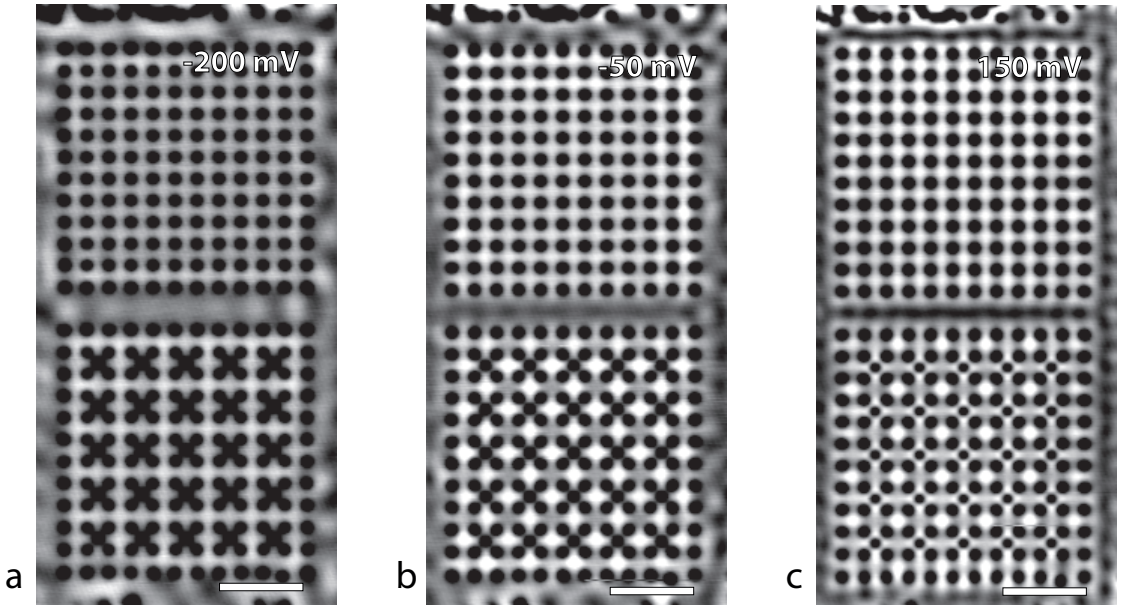

Figure 12: Differential conductance maps at various bias voltages, (**a**) -200 mV, (**b**) -50 mV and (**c**) 150 mV, all with a scale bar of 5 nm. The maps were taken on a Lieb lattice with a square lattice of similar dimensions built next to it as a reference lattice. The full series of maps can be seen in the Appendix Figure 20.

on the edge sites while the upper and lower bands contains states located on both corner and edge sites where the corner sites are more dominant. Figure 12a shows the lower band which will converge into the Dirac cone situated around -200 mV where the corner sites have a larger intensity than the edge sites. This corresponds to the lowest band of the density of states calculated from tight-binding calculations, shown in Figure 1c and d in the Theory. In Figure 12b the map taken at -50 mV is shown where there is high intensity at the edge sites and much less at the corner sites. This corresponds to the flat band intersecting the Dirac cone at the Fermi energy. Figure 12c shows the upper band at a higher energy (150 mV) than the flat band. Here the edge sites have much less intensity than the corner sites. Also one can see higher orders of the band structure emerging within the inverse Lieb lattice block. Higher-energy effects are quite visible in the bandstructure in the maps from 200 mV onwards, shown in Appendix 20. These higher order effects are explained in section 4.5.

The three maps represent the Lieb electronic structure very well, however the energy spacing between the maps was rather large at 50 mV.

4.4 Influence of unit cell size

As shown in Figure 13 there is a large influence of the unit cell size on the position of the peaks in spectra measured on the Lieb lattices, which is also shown by Gomes *et al.* for molecular graphene [9]. The differently-sized lattices are shown in (a)–(c) going from

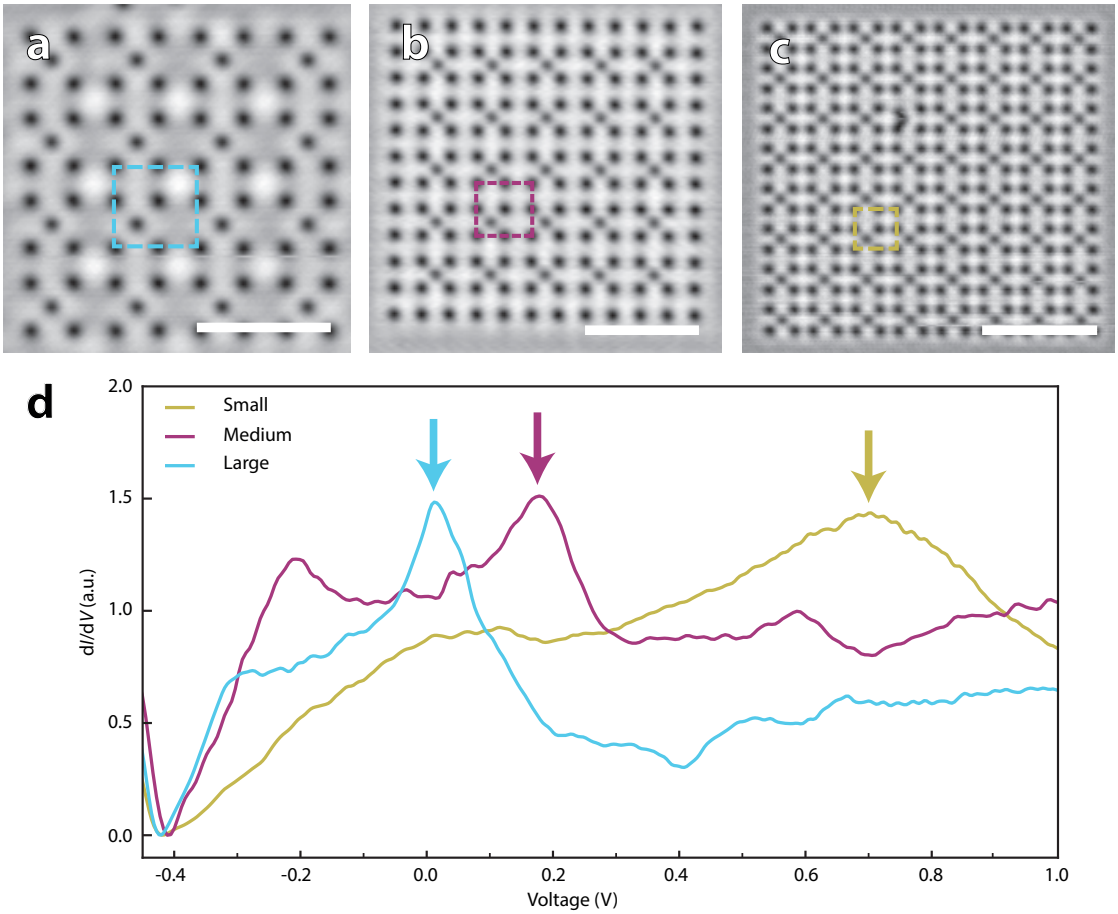

Figure 13: Three inverse Lieb lattices built with different unit cell sizes. All scale bars are 5 nm. (**a**) 4 by 4 lattice with a unit cell size of 3.06 x 3.09 nm (red). (**b**) 5 by 5 lattice with a unit cell size of 2.66 x 2.56 nm (blue). (**c**) 8 by 8 lattice with a unit cell size of 1.76 x 1.79 nm (green). (**d**) Spectra taken on the corner sites of three different sizes of Lieb lattices varying from 1.76 x 1.79 nm (green) to 2.66 x 2.55 nm (blue) to 3.06 x 3.09 nm (red). The arrows indicate the peaks of interest.

a large unit cell to a small unit cell. For a small unit cell size of a Lieb lattice of 1.76 x 1.79 nm (blue) the right hand peak of the Dirac cone is located around 700 mV while for a lattice with a unit cell nearly twice as large (3.06 x 3.09 nm in red) the same peak is only just higher than 0 mV. This is a large shift, but in the same range of order as Gomes *et al.* found when changing lattice parameters. The shifting of the bands is due to a larger degree of confinement of the surface state electrons. The less space they have, the higher in energy the band structure becomes [40]. Further measurements should definitely be performed to quantitatively check the influence of spacing of the unit cells, the spacing of the CO molecules within the unit cell and if the energy shifts are comparable to those in molecular graphene. Another aspect which can be noticed in the size-dependent spectra

Lattice	Unit cell ratio (c_h/c_v)	horizontal ratio (a_h/b_h)	vertical ratio (a_v/b_v)
Large	1.01	1.33	1.00
Medium	1.04	1.00	1.00
Small	0.99	1.00	1.33

Table 1: Ratios of various lattice size unit cells determining the equivalency of various dimensions.

is the peak width: a decrease in unit cell size increases the peak width. This effect is assigned to coupling of the energy bands to bulk Cu states [41].

For clarity of Figure 13 only spectra taken on corner sites are shown although spectra on edge sites show an identical trend. The various unit cell sizes were built and measured with different tips and therefore the spectra do not all have the same shape. The Lieb signature is however still always visible, further consolidating our results.

The shifting of the bands to higher or lower energies generates a type of doping. Doping a system means adding either more electrons (n-doping) or less electrons (p-doping) to a system [9]. Because we are building a lattice on a steady Cu surface state we cannot change the amount of electrons while we can change the size of the system, or unit cell, which contains electrons. The Fermi energy of the Cu surface state is fixed at 0 V so the medium unit cell size in Figure 13b is filled to the middle of the two bands contributing to a Dirac cone shape yielding a relatively neutral system. By enlarging the system the bands shift to lower energies. As the Fermi energy of the electrons stays at 0 V the system is now filled to the upper band. When decreasing the unit cell size the bands shift to higher energies meaning that they will only be filled to the bottom band. By tuning the system size one can thus tune the electronic stucture.

So in theory, any unit cell size and shape can thus be chosen and the peaks will shift accordingly. However, the size of the unit cell also implicitly influences the positioning of the CO molecules in real space on the Cu(111) crystal. Because there is a limitation to placing CO molecules on the top sites of the copper surface, geometry issues start to play a role when creating small unit cell sizes. One can see a small asymmetry within the small lattice unit cell in Figure 13c as the width of the CO cross shape is larger than the height. For the large unit cell (Figure 13a) it is vice versa, the height is larger than the width. This illustrates the problems of building a square lattice on a hexagonal substrate, it is nearly impossible especially on a small scale. This is illustrated in a schematic way in Figure 14. Here one can see the positioning of CO molecules to create three different sized unit cells and the interior dimensions. The CO molecules are portrayed by red circles positioned on top sites of the Cu(111) surface (light yellow), while the unit cells are indicated by dashed squares. The ratios of these dimensions (a_h - c_v) are gathered in Table 1 for comparison. When the horizontal and vertical ratios are equal to 1.00 the edge sites are of equal shape and size as is the case for the medium lattice (2.66 x 2.56 nm). The medium lattice has a larger error in the unit cell ratio, but the edge sites are equally shaped which is more important as shown in the next paragraph. Also the error in unit cell ratio is only 4% which is not large.

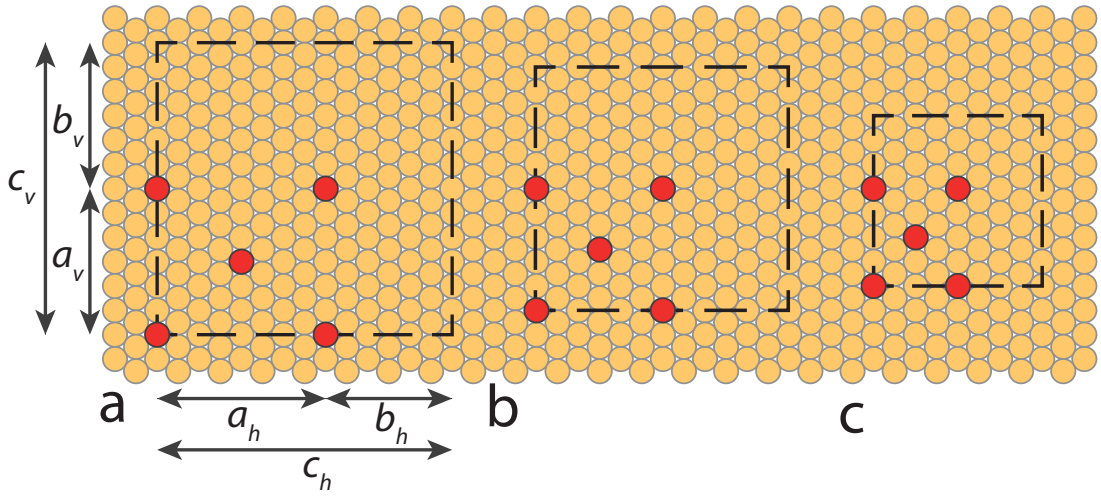

Figure 14: Schematic representation of various sizes and the relative dimensions of and within the unit cells of the Lieb lattices. CO molecules are represented in red with the Cu(111) surface in light yellow with a nearest neighbour distance of 0.2556 nm. **(a)** 3.09 x 3.06 nm unit cell. **(b)** 2.66 x 2.56 nm unit cell. **(c)** 1.77 x 1.79 nm unit cell.

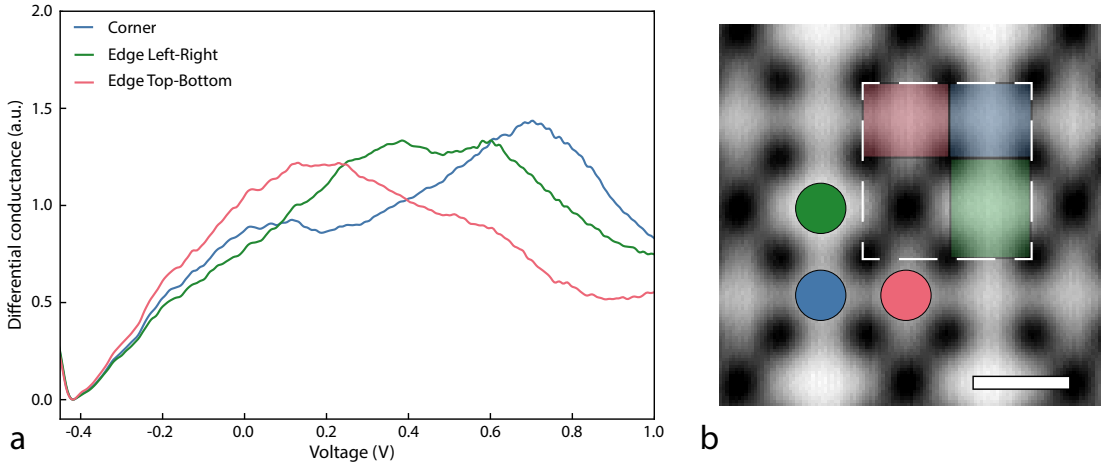

Figure 15: **(a)** Spectra taken on the small lattice with a unit cell of 1.77 x 1.79 nm with corner spectra in blue, edge spectra bordered by the CO molecules on the top and bottom in green and edge spectra bordered on the left and right in red. **(b)** STM image taken at 1 nA and 50 mV with the unit cell indicated by the white dashed square, corner sites (blue), edge sites bordered on the top and bottom (green) and edge sites bordered on the left and right (red). The scale bar is 1 nm.

The importance of having equally shaped edge sites is shown in Figure 15. In this lattice the horizontal and vertical ratios are 1.00 and 1.33 respectively. This means that the dimensions of the edge sites are not equivalent. The asymmetry of the edge sites

is due to the differing degrees of confinement by the CO molecules. The effect of this inequivalency is shown by the spectra in Figure 15. When the confinement is larger, i.e. the edge site is smaller, the spectrum shifts to higher energy. This is analogous to the unit cell size effect described earlier. The difference of confinement is only a few Å and shows just how subtle the interplay is between unit cell size and unit cell symmetry.

To remove this clearly unwanted effect of inequivalent sites, one must adjust the spacing of the CO molecules to create an equivalency of edge sites while maintaining an (almost) square unit cell. An optimum configuration was found using the unit cell size of 2.66 x 2.56 nm.

4.5 Higher-energy effects

The maps shown earlier in section 4.3 are not the only maps of interest when looking at higher-energy effects in the Lieb and square lattice. The map at 150 mV (Figure 12c) showed extra sites forming in the CO cross of the Lieb lattice. To visualise the effects on the LDOS better one can look at the differential conductance maps at a higher energy such as in Figure 16a, a map taken at 550 mV. Here one can see that the corner sites in the square lattice have diminished so much in intensity they have a similar contrast as CO molecules while the bridge sites now have high intensity in contrast to the maps seen earlier in Figure 12. A few real CO molecules have been marked with a yellow circle to help guide the eye. The intensity pattern of the sites surrounding the CO molecule bears a huge resemblance with the intensity pattern produced by the 'standard' Lieb lattice measured at the resonance of the flat band shown in the bottom of Figure 12b. In both cases the sides of a Lieb lattice unit cell have been split into 3 sites of which the central one has a high intensity and the two outer corner sites have a lower intensity.

A similar effect occurs in the Lieb lattice when going from -50 mV to 550 mV. The edge sites where there was high intensity at -50 mV become low intensity sites at 550 mV while the corner sites stay at low intensity. The bridge sites which acted as nodal sites in Figure 12b become high intensity sites in Figure 16a. This means there are now 5 sites along one length of a Lieb unit cell and 11 sites within the unit cell (white dashed square) in comparison with the 3 in the standard Lieb lattice.

These higher order effects can be explained in a schematic figure with various sites and how they can be made by placement of CO molecules. This is done in Figure 16b–i. A square lattice consists of one site per unit cell as depicted in (b). It can be created by CO molecules on Cu(111) by placing a single CO molecule in the centre of the square unit cell (g). If one includes the 'bridge' sites as seen in the top half of (a) then you get 3 sites per unit cell (c). A unit cell with three sites is actually a Lieb lattice as shown in (d). The Lieb lattice can (as shown earlier) be built by a cross shape of 5 CO molecules (h). If we repeat the process, but then with the Lieb unit cell, including the extra 'bridge' sites (e) we end up with a superlieb structure with 11 sites per unit cell (f). If we compare the pseudo-superlieb structure from (e) to the intensities in the bottom half of (a) we can see that a higher order of the Lieb lattice is a pseudo-superlieb lattice. Both have 5 sites per side of the unit cell where blue circles correspond to low intensity and red circles correspond to high intensity. A superlieb lattice could be made

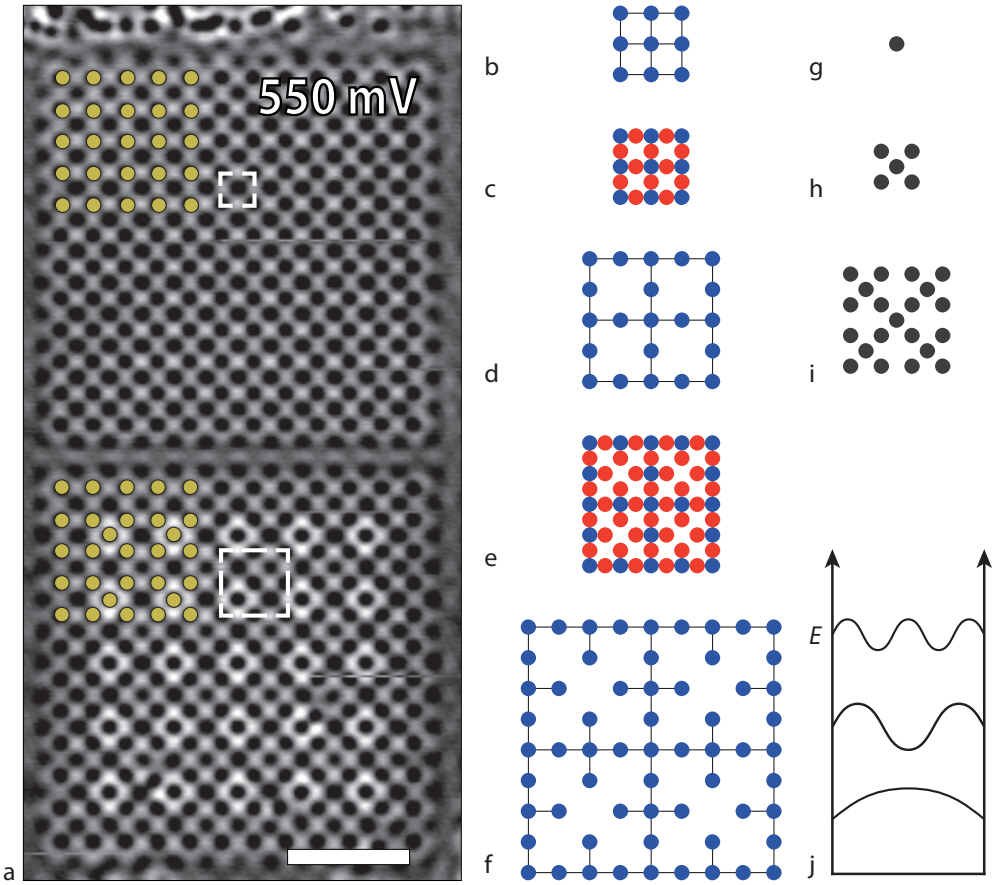

Figure 16: Schematic representation of higher order states going from square to Lieb to superlieb structures. **(a)** Differential conductance map of a square (top) and Lieb (bottom) lattice taken at 550 mV with the CO molecules marked by yellow circles to guide the eye. The unit cells are indicated by the white dashed square. The scale bar is 5 nm.**(b)** 2 by 2 square lattice with the single site per unit cell in blue. **(c)** 2 by 2 square lattice with interstitial sites in red forming a Lieb lattice with 3 sites per unit cell. **(d)** 2 by 2 Lieb lattice with the sites in blue. **(e)** 2 by 2 Lieb lattice with interstitial sites in red forming a superlieb lattice with 11 sites per unit cell. **(f)** 2 by 2 superlieb lattice with the sites in blue. **(g)** Single CO molecule used to create the square lattice in (b) **(h)** Cross arrangement of 5 CO molecules used to create the Lieb lattice in (d) **(i)** Advanced cross arrangement of 21 CO molecules used to create a superlieb lattice in (f). **(j)** Sketch indicating waves with an increasing amount of antinodes from bottom to top going from 1 to 3 to 5.

by combining four CO crosses with a central CO molecule, much like the CO cross is formed by 4 CO molecules with a central one.

When measuring at higher energies one thus encounters higher order states which

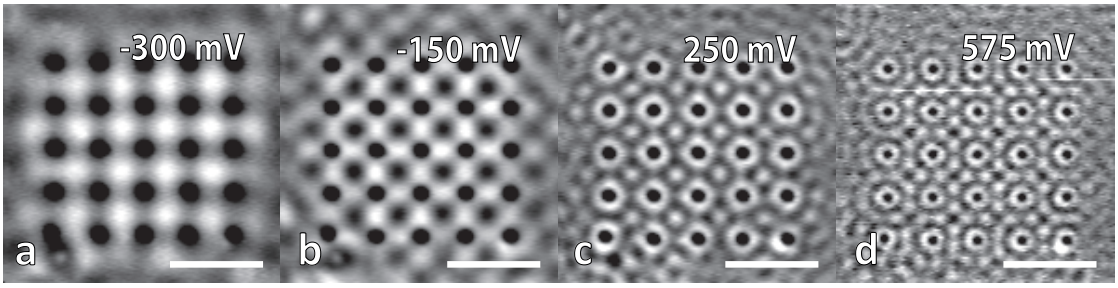

Figure 17: Differential conductance maps taken on a large square lattice with a unit cell of 2.66 by 2.56 nm visualising higher order effects **(a)** Map taken at -300 mV with high intensity at corner sites. **(b)** Map taken at -150 mV with low intensity at the corner sites and high intensity at 'edge' sites. **(c)** Map taken at 250 mV with high intensity at the corner sites, a slight intensity at the 'edge' sites and low intensity at 'bridge' sites. **(d)** Map taken at 575 mV with high intensity at the 'bridge' sites and low intensity at the corner and 'edge' sites. All scale bars are 5 nm

are similar to the ground states, but then with more nodal planes. One can compare it to Figure 16j where a comparison in 1D is drawn. Gaining in energy a wavefunction will have more antinodes going from 1 to 3 to 5 when going from bottom to top. The increase of nodes at higher energies is similar to the particle in a box model [40] where wavefunctions with n more nodes increase the energy of the wave with n^2.

The results we find in the differential conductance maps are in agreement with the results we obtained earlier on unit cell size-effects. In the case of the square lattice the unit cell is half the dimensions of the Lieb unit cell and therefore it is not unexpected that the higher energy states of a square lattice would be occurring at higher energies than the Lieb effects occuring in the Lieb lattice do. Taking this comparison further we would expect the higher energy states of a square lattice with the same unit cell size of the Lieb lattice (2.66 x2.56 nm) would occur at lower energies.

In Figure 17 one can see four differential conductance maps on a large square lattice with a unit cell of exactly the same dimensions as the Lieb lattice in Figure 16. In (a) a map taken at -300 mV is shown where corner sites have a high intensity and the bridge sites (or 'edge' sites) have a low intensity similar to the LDOS of the lower band of the Lieb lattice. (b) Shows a flipping of intensities, where the bridge sites start acting as edge sites would in a Lieb lattice. It forms a quasi-Lieb lattice where the edge sites have a higher intensity than the corner sites corresponding to the flat band. Still increasing the energy we arrive at 250 mV (c). Here one sees that the three site model of (a) and (b) no longer suffices to describe the intensity spacing. The corner sites have the highest intensity followed by the edge sites. The secondary bridge sites in between the corner and edge sites have a low intensity. The eleven site model proposed in Figure 16(e and f) is not totally applicable as with the square lattice there is only one CO molecule per unit cell. Due to the absence of the 4 extra CO molecules, the eleven site model does not describe the available sites for the electrons any more. A map taken at 575 mV (d)

shows the large square where the intensities have changed again, the corner and edge sites are low intensity while the secondary bridge sites have a high intensity. This effect is also found in the centre of the unit cell, not only along the sides, which explains the high intensity located immediately around the CO molecule.

These patterns correspond neatly to the results we obtained in the Lieb and smaller square lattice while also proving the shift of the enegries of the bands when changing lattice parameters.

The fact that we see the Lieb signatures in all spectra visualisation techniques is a strong supporting argument that our configuration of five CO molecules per unit cell modifying the 2DEG of Cu(111) actually generates an electronic Lieb lattice. In all measurements on the artificial Lieb lattice the Lieb signature, a flat band and two bands converging into a Dirac cone as explained in the theory, can be seen. All spectra taken on edge sites show a density of states corresponding to a flat band while spectra taken on corner sites have two prominent peaks due to the Dirac cone being formed.

5 Conclusion

An artificial electronic Lieb lattice was created by atomically precise manipulations of CO molecules on a Cu(111) substrate leading to sub nano-scale patterning of the two-dimensional electron gas at the surface of the Cu crystal. Differential conductance spectra were taken at the three sites within a unit cell of the Lieb lattice. The spectra correspond to the theoretical shape of the density of states where the edge sites in the Lieb lattice have a high intensity round the Fermi energy and the corner sites have high intensity at the energies corresponding to the top and bottom band of the theoretical band structure. There are finite-size effects present as the measurements were performed on a 5 by 5 unit cell lattice. This causes an extra peak in the edge spectrum. The effect on the spectra by changing the unit cell dimensions was investigated showing possibilities to dope a Lieb lattice simply by changing the unit cell size. Higher-energy effects have been studied in the Lieb lattice and a large square lattice showing the existence of a pseudo super-Lieb lattice in a Lieb lattice when imaging at higher energies. The line spectra, differential conductance maps and higher energy states all correspond to the expected theoretical predictions. Together they all indicate that we have created an artificial electronic Lieb lattice on Cu(111) by atomically precise positioning of CO molecules leading to modification of the 2DEG on the surface of Cu.

6 Outlook

The measurements in this thesis have shown that one can create artificial structures with Dirac cones and a flat band. These characteristics are a very hot topic at the moment especially as the Nobel Prize for Physics 2016 was awarded for topological phases which a really flat band would be categorised as. We would like to continue the research on these artificial lattices and investigate ways to manipulate the band structure shapes. Creating the honeycomb lattices that Gomes *et al.* did [9] extends the range of lattices to work with. The effect of inducing defects in such lattices is very interesting as they induce local changes in the electronic structure. Combining these effects with superconductivity, spin-orbit coupling, and edge effects in various 2D lattices and substrates will generate a nearly limitless amount of ideas to work on.

To consolidate our knowledge of the effect of unit cell and spacing lengths, I suggest that we do a short but comprehensive comparison of various sizes of Lieb lattices and graphene and measure them all with the same tip. This could be achieved by building a large array of various sized, spaced and types of lattices near each other and measuring them with a constant tip. Due to the finite-size effects on the spectra a logical step is to create larger artificial electronic Lieb lattices. Building 10 by 10 unit cell lattices or even larger would definitely diminish the peak due to finite-size found in the spectra. Artificial electronic lattices have all the properties of a real lattice save the ability to be picked up and viewed under an optical microscope. Using the techniques we have shown in this thesis, one could easily build many more 2D systems, lattices or molecules that simply have not been able to be investigated in the past due to the type of lattice not existing in nature. Based on the similarity of the higher-order effects to fractal patterns, the construction of fractal lattices such as a Sierpinski carpet [42], which could be seen as a Lieb lattice of Lieb lattices, could yield very interesting band structures, besides being aesthetically pleasing.

The research in this thesis is quite fundamental and will never be used as is in any consumer product any time soon. In 2002 though, the possibilities to use CO molecules in logic circuits was shown by Heinrich *et al.* [43]. He created molecular cascades of CO molecules which could thereby perform simple and/or comparisons. This shows just how versatile a 'simple' system of CO molecules on a Cu(111) surface can be.

Once we have SnapZone working efficiently and reliably nearly any pattern or lattice can be designed, built and immediately measured, enabling a relatively high-throughput for measurements. Manual manipulation is really only exciting for so many manipulations, and automation can also utilise general down-time such as nights and weekends. This would definitely increase the effective usage time of the STM's and be one step further in the automation of our set-up.

I am confident that with some hard work in the next few years we will be able to say:

You name it, we build it.

Acknowledgements

A certain tour through the labs at CMI during which I encountered the large brushed stainless steel vacuum chambers located in the basement convinced me to work with this awe-inspiring apparatus during my master. One and a half amazing years later I still enjoy their presence and abilities. Although I chose my project based on machinery, people still influence research a lot more.

I would like to sincerely thank *Marlou* as my daily supervisor for all her help during my master's thesis. No matter what, you would check that everything was still going well at least once a day. Also I would like to thank *Ingmar* for giving me the opportunity to do my master's thesis in his basement group, and for the chats with him while biking home. The other PhD candidates in the *Basement Group*: Joost, Nadine, Jaco and Peter helped welcome me into the group, taught me the basics (and more) of our LT-STM set-up, how to analyse my data and made for very nice Monday morning meetings!

I have also been introduced to the awesome programming language Python which I have learned, mainly by fiddling around with bits of code, to use in the last one and a half years. Many thanks go to *Stephan* for his work on SnapZone, I really hope it can be put to good use soon!

Without theory experiments simply do not make sense, so I would like to thank Guido, Sander and Christiane from the *Institute for Theoretical Physics* for the calculations and discussions even if some of it went far over my head.

Research would stagnate if you cannot have some fun once in a while and that is what I would like to thank CMI, and the master students in particular, for. Everybody is interested in each others work, and helps keep the general atmosphere enjoyable.

References

[1] K. S. Novoselov, A. K. Geim, S. V. Morozov, D. Jiang, Y. Zhang, S. V. Dubonos, I. V. Grigorieva and A. Firsov. *Science 306*, (2004), 666–669.

[2] S. G. Louie and C. H. Park. *Nano Letters 9*, (2009), 1793–1797.

[3] M. Nita, B. Ostahie and A. Aldea. *Physical Review B 87*, (2013), 125428.

[4] W. Häusler. *Physical Review B 91*, (2015), 1–5.

[5] W. Beugeling, J. C. Everts and C. Morais Smith. *Physical Review B 86*, (2012), 195129.

[6] R. Shen, L. B. Shao, B. Wang and D. Y. Xing. *Physical Review B - Condensed Matter and Materials Physics 81*, (2010), 2–5.

[7] N. Goldman, D. F. Urban and D. Bercioux. *Physical Review A 83, (2011).*

[8] S. Mukherjee, A. Spracklen, D. Choudhury, N. Goldman, P. Öhberg, E. Andersson and R. R. Thomson. *Physical Review Letters 114*, (2015), 1–5.

[9] K. K. Gomes, W. Mar, W. Ko, F. Guinea and H. C. Manoharan. *Nature 483*, (2012), 306–310.

[10] L. Bartels, G. Meyer and K. H. Rieder. *Chemical Physics Letters 273*, (1997), 371–375.

[11] J. A. Stroscio and R. J. Celotta. *Science (New York, N.Y.) 306*, (2004), 242–7.

[12] A. Floris, A. Sanna, S. Massidda and E. K. U. Gross. *Physical Review B - Condensed Matter and Materials Physics 75*, (2007), 1–6.

[13] V. Galitski and I. B. Spielman. *Nature 494*, (2013), 49–54.

[14] H. L. Störmer. The fractional quantum Hall effect, **1998**.

[15] J. D. Gouveia and R. G. Dias. *ArXiv[1505.01656]* .

[16] I. Swart. Lecture notes from 'Solids and Surfaces' course at Utrecht University, **2016**.

[17] A. K. Geim and K. S. Novoselov. *Nature materials 6*, (2007), 183–91.

[18] M. R. Slot, T. S. Gardenier, P. H. Jacobse, G. C. P. van Miert, S. N. Kempkes, S. J. M. Zevenhuizen, C. M. Smith, D. Vanmaekelbergh and I. Swart. *ArXiv[1611.04641]* 1–37.

[19] C. Weeks and M. Franz. *Physical Review B - Condensed Matter and Materials Physics 82.*

[20] W.-X. Qiu, S. Li, J.-H. Gao, Y. Zhou and F.-C. Zhang. *ArXiv[1609.01876]* 1–5.

[21] R. A. Vicencio, C. Cantillano, L. Morales-Inostroza, B. Real, C. Mejía-Cortés, S. Weimann, A. Szameit and M. I. Molina. *Physical Review Letters 114*, (2015), 1–5.

[22] G. Binnig, H. Rohrer, C. Gerber and E. Weibel. *Physical review letters 49*, (1982), 57–61.

[23] S. Kano, T. Tada and Y. Majima. *Chem. Soc. Rev. 44*, (2015), 970–987.

[24] P. Roushan. *Visualizing surface states of topological insulators with scanning tunneling microscopy*. Ph.D. thesis, Princeton University, **2011**.

[25] C. J. Chen. *Introduction to Scanning Tunneling Microscopy*. Oxford University Press Inc., New York, second edition, **2008**.

[26] G. Hörmandinger. *Physical Review B 49*, (1994), 13897–13905.

[27] W. Shockley. *Physical Review 56*, (1939), 317–323.

[28] E. J. Heller, M. F. Crommie, C. P. Lutz and D. M. Eigler. *Nature 369*, (1994), 464–466.

[29] K.-F. Braun and K.-H. Rieder. *Physical review letters 88*, (2002), 096801.

[30] D. K. Schweizer and E. K. Eigler. Positioning single atoms with a scanning tunneling microscop, **1990**.

[31] R. J. Celotta, S. B. Balakirsky, A. P. Fein, F. M. Hess, G. M. Rutter and J. a. Stroscio. *Review of Scientific Instruments 85*, (2014), 121301.

[32] F. Besenbacher. *Reports on Progress in Physics 59*, (1996), 1737–1802.

[33] R. I. Dekker and T. S. Gardenier. A first-principles DFT study on an artificial molecular Lieb lattice. Technical Report June, Utrecht University, Utrecht, **2016**.

[34] M. Ropo, S. Paavilainen, J. Akola and E. Räsänen. *Physical Review B - Condensed Matter and Materials Physics 90*, (2014), 1–5.

[35] S. Paavilainen, M. Ropo, J. Nieminen, J. Akola and E. Räsänen. *Nano Letters 16*, (2016), 3519–3523.

[36] G. Meyer, S. Zöphel and K. H. Rieder. *Applied Physics A Materials Science and Processing 63*, (1996), 557–564.

[37] G. Meyer, L. Bartels and K. H. Rieder. *Computational Materials Science 20*, (2001), 443–450.

[38] W. M. Haynes, editor. *Handbook of Chemistry and Physics*. CRC Press, 91 edition, **2010**.

[39] J. Li, W.-D. Schneider, R. Berndt, O. Bryant and S. Crampin. *Physical Review Letters 81*, (1998), 4464–4467.

[40] D. Ball. *Physical Chemistry*. Cengage Learning, Inc, 1 edition, **2003**.

[41] S. Crampin, M. H. Boon and J. E. Inglesfield. *Physical Review Letters 73*, (1994), 1015–1018.

[42] M. T. Barlow and R. F. Bass. *Canadian Journal of Mathematics 51*, (1999), 673–744.

[43] A. J. Heinrich. *Science 298*, (2002), 1381–1387.

Appendix

Spectroscopy results for other tips

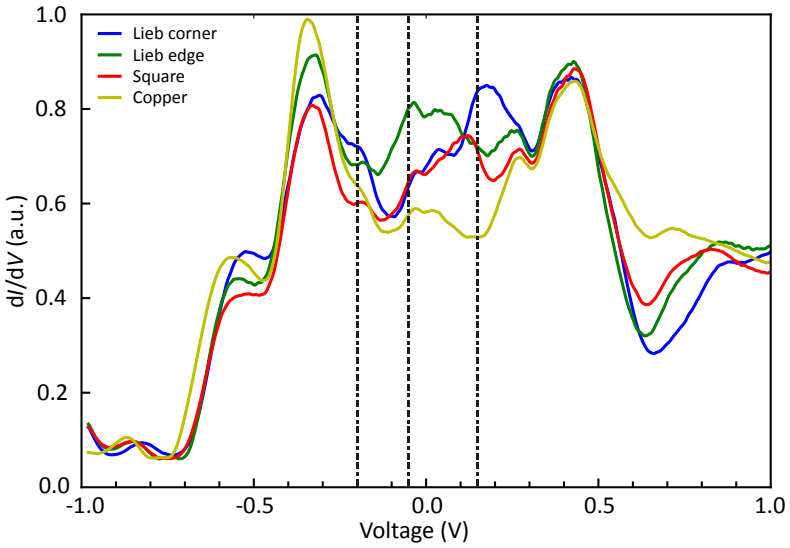

Figure 18: Spectrocopy taken on a 5 by 5 inverse Lieb lattice similar to the lattice used in Figure 9. The tip however has a significantly different configuration indicated by the Cu spectrum in yellow. Also the surface state onset around -0.45 V is not a sharp transition. The Lieb signature is however slightly clearer than in Figure 9. The dashed lines indicate the energies of interest (-200 mV, -50 mV, 150 mV) where the corner and edge sites have different intensities.

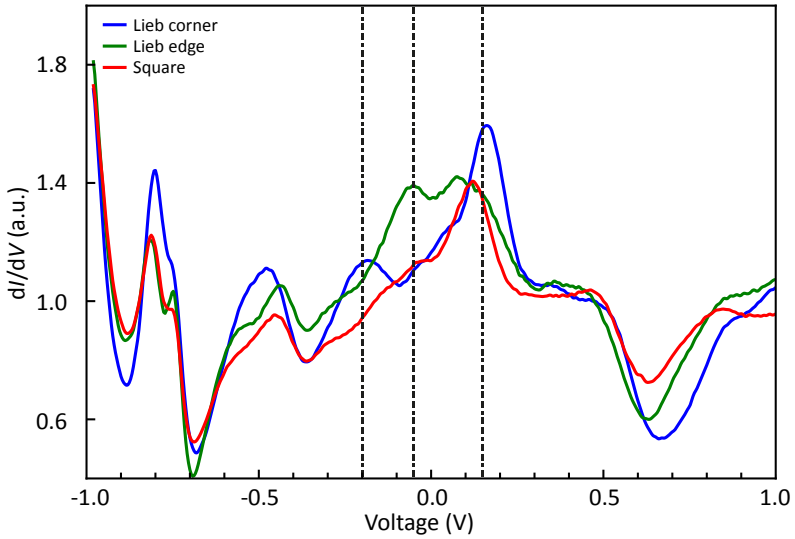

Figure 19: Spectroscopy taken with the same tip as 18 and divided by the CU spectrum. The Lieb signature is a lot clearer in this Figure. Here one sees the corner spectra in blue with high intensities at -200 mV and 150 mV and the edge spectra with high intensity around -50 mV and the extra peak due to finite-size effects around 75 mV. The spectra taken on the square lattice show no remarkable features in this energy range due to a fairly constant increase in the intensity, which you could see as a background intensity.

Differential conductance map series

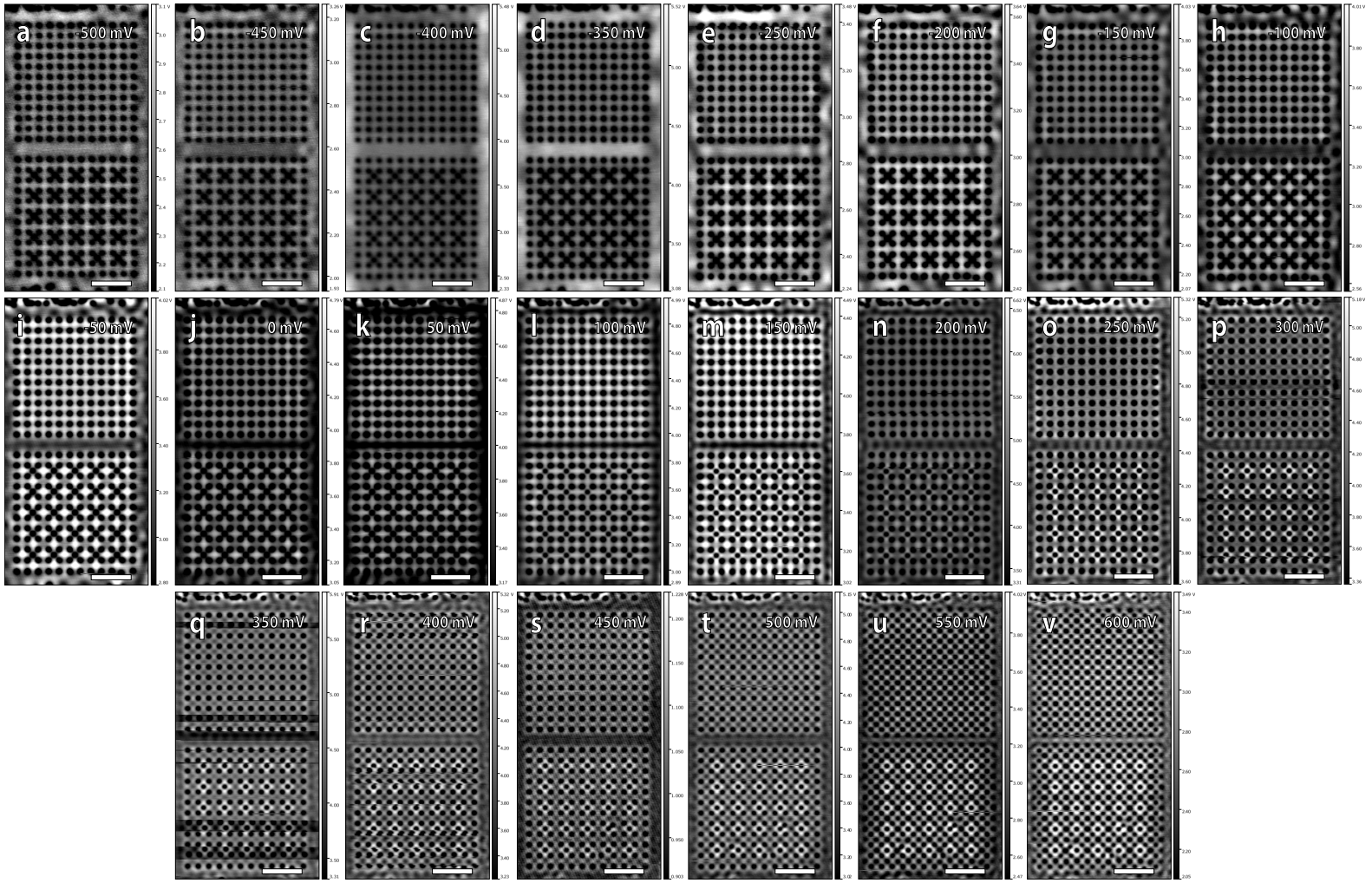

Figure 20: The differential conductance map set at (**a**) -500 mV (**b**) -450 mV (**c**) -400 mV (**d**) -350 mV (**e**) -250 mV (**f**) -200 mV (**g**) -150 mV (**h**) -100 mV (**i**) -50 mV (**j**) 0 mV (**k**) 50 mV (**l**) 100 mV (**m**) 150 mV (**n**) 200 mV (**o**) 250 mV (**p**) 300 mV (**q**) 350 mV (**r**) 400 mV (**s**) 450 mV (**t**) 500 mV (**u**) 550 mV (**v**) 600 mV. The map at -300 mV is not included due to to an insufficiently consistent contrast throughout the total image.